Available online at www.sciencedirect.com
ScienceDirect
Trans. Nonferrous Met. Soc. China 27(2017) 1105−1116
Transactions of Nonferrous Metals Society of China
www.tnmsc.cn

Hydrothermal synthesis and electrochemical sensing properties of copper vanadate nanocrystals with controlled morphologies

Gui-hong HAN[1], Shu-zhen YANG[1], Yan-fang HUANG[1], Jing YANG[2], Wen-cui CHAI[1], Rui ZHANG[2], De-liang CHEN[2]

1. School of Chemical Engineering and Energy, Zhengzhou University, Zhengzhou 450001, China;
2. School of Materials Science and Engineering, Zhengzhou University, Zhengzhou 450001, China

Received 12 March 2016; accepted 1 September 2016

Abstract: Morphology-controlled synthesis of copper vanadate nanocrystals is of great significance in electrochemical sensing applications. A facile hydrothermal process for synthesizing copper vanadate nanocrystals with various morphologies (e.g., nanoparticles, nanobelts and nanoflowers) was reported. Phase, morphology and electrochemical performance of the as-synthesized copper vanadate nanocrystals were characterized by X-ray diffraction (XRD), scanning electron microscope (SEM) and cyclic-voltammogram (CV) techniques. The results revealed that the morphologies of the $Cu_3V_2O_7(OH)_2{\cdot}2H_2O$ (CVOH) nanocrystals could be controlled by changing copper salts, surfactants and pH values. The CVOH samples showed enhanced electrochemical response to ascorbic acid. Comparatively, the CVOH nanobelts had the higher electrochemical sensing performance than those of CVOH nanoparticles and nanoflowers. The CVOH-nanobelts-modified GCEs had a linear relationship between the peak currents in their CVs and ascorbic acid concentration. The CVOH nanocrystals can be used as potential electrochemical active materials for the determination of ascorbic acid.

Key words: copper vanadate nanocrystals; hydrothermal synthesis; electrochemical sensors; ascorbic acid

1 Introduction

Ascorbic acid (AA) is one of the most important vitamins due to its antioxidant and other benefits for human bodies [1]. AA is often added to various foods and pharmaceutical products for prevention of some diseases. The detection and quantitative determination of AA for the quality control in producing pharmaceuticals is essentially important. Therefore, there is an urgent need in developing easy-to-use and inexpensive methods to detect AA [2]. Electrochemical methods for accurate determination of analytes have attracted increasing attention because of their intrinsic advantages of rapid response, high sensitivity, easy operation and low cost [3]. Glassy carbon electrodes (GCE), carbon paste (CP) electrodes and gold arrays microelectrodes, which were functionalized by various active materials, have been used to detect various analytes [4−6]. Nanocrystals of metal oxides, carbon and metals were widely used to modify the electrodes' surfaces to facilitate the electron transfer between target analytes and electrode surfaces and then to improve their performance [7−12]. The morphologies and sizes of the nanocrystals highly affect the modification [13] and electrochemical property of electrodes [7]. Metal vanadate nanocrystals have been reported in electrochemical applications [14−18]. Among those metal vanadates, copper vanadate nanocrystals showed a great potential in the surface modification of electrodes because of their unique electrochemical performance [11,16].

Controlled synthesis and electrochemical applications of copper vanadate nanocrystals with unique morphologies and sizes are the most interesting research topics. Their electrochemical properties are highly influenced by the morphologies and sizes that are largely determined by synthetic processes and starting reactants. As a typical phase, CuV_2O_6 nanocrystals have been

Foundation item: Projects (51404213, 51404214, 51574205, 51172211) supported by the National Natural Science Foundation of China; Projects (14HASTIT011, 154100510003) supported by the Program for University Science and Technology Innovation Talents of Henan Province, China; Projects (2013M531682, 2014T70682) supported by the China Postdoctoral Science Fund; Project (1421324065) supported by the Development Fund for Outstanding Young Teachers of Zhengzhou University, China
Corresponding author: De-liang CHEN; Tel: +86-371+67881046; Fax: +86-371+67881593; E-mail: dlchen@zzu.edu.cn
DOI: 10.1016/S1003-6326(17)60129-8

synthesized via various processes (i.e., solid-state reaction, sol-gel process, hydrothermal method) using different starting materials (i.e., V_2O_5 + $Cu(NO_3)_2$ [19], NH_4VO_3 + $Cu(NO_3)_2$ [20], V_2O_5 hydrogel + Cu_2O [21]). Hollow $Cu_{0.95}V_2O_5$ microspheres and CuV_2O_6 nanoparticles have been synthesized using VO_2 and $Cu(NO_3)_2$ as precursors in the polyvinyl pyrrollidone solutions [22]. Also, $Cu_2V_2O_7$ nanoparticles have been synthesized using a thermal-decomposition method [11]. Recently, $Cu_3(OH)_2V_2O_7{\cdot}nH_2O$ nanoparticles have been synthesized by hydrothermal methods using V_2O_5 + $Cu(NO_3)_2$ [23] or V_2O_5 + $CuSO_4{\cdot}7H_2O$ [24] as the starting materials. $Cu_3(OH)_2V_2O_7{\cdot}2H_2O$ samples with different morphologies and sizes by a sol-gel process or chemical precipitation method were also reported [25,26]. In addition, $Cu_3V_2O_8$ nanoparticles have been gotten with $CuSO_4{\cdot}5H_2O$ and NH_4VO_3 as materials under the assistance of different Schiff base ligands via a simple precipitation approach [27,28]. However, the synthesis of copper vanadate nanocrystals with controlled morphologies using simple and cost-effective methods is still full of challenges.

In this work, a new and facile hydrothermal process was developed to synthesize copper vanadate nanomaterials with various morphologies, and their applications in electrochemical detection of AA were systematically investigated. The optimal hydrothermal conditions were explored by adjusting acid radicals, additives and pH values, which are the key factors affecting the morphologies [29−32]. The copper vanadate nanocrystals with typically unique morphologies (i.e., nanoparticles, nanobelts, and nanoflowers) have been used as the active materials to modify GCEs, which were used as the working electrodes to detect ascorbic acid on the basis of the electrochemically sensing mechanism.

2 Experimental

2.1 Materials and methods

NH_4VO_3 (AR grade) and $Cu(CH_3COO)_2{\cdot}H_2O$ (AR grade) were purchased from Tianjin Guangfu Fine Chemical Research, China. $CuSO_4{\cdot}5H_2O$ (AR grade, Tianjin Kemiou Chemical Reagent Co., Ltd, China), $CuCl_2{\cdot}H_2O$ (AR grade, Tianjin Fengchuan Chemical Reagent Co., Ltd., China) were also used as copper sources. $Cu(NO_3)_2{\cdot}3H_2O$ (AR grade) and polyvinylpyrrolidone (PVP) were obtained from Sinopharm Chemical Reagent Co., Ltd., sodium dodecyl benzene sulfonate (SDBS) and hexadecyltrimethy ammonium bromide (CTAB) were purchased from Tianjin Fu Chen Chemical Reagents Factory and China National Pharmaceutical Group Corporation, respectively. All chemicals were used as received.

Copper vanadate samples were synthesized under different conditions, by varying copper sources ($CuSO_4$, $Cu(NO_3)_2$, $Cu(CH_3COO)_2$, or $CuCl_2$), Cu^{2+} concentration (0.03−0.075 mol/L), surfactants (PVP, SDBS or CTAB), pH values (3−11) and hydrothermal reaction time (12−24 h). The details for hydrothermal synthesis of copper vanadate nanocrystals are listed in Table 1.

In a typical synthesis (S6 in Table 1), 0.1404 g (~1.2 mmol) of NH_4VO_3 was dissolved in 30 mL of distilled water at 80 °C under magnetic stirring, and

Table 1 Summary of experimental parameters for hydrothermal synthesis of copper vanadate nanocrystals

Sample No.	Copper source	Cu^{2+} concentration/ ($mol{\cdot}L^{-1}$)	Surfactant/ concentration/%	Time/h	pH	Morphology of products
S1	$CuSO_4$	0.03	PVP / 2.7	24	4	Nanoflowers
S2	$CuSO_4$	0.03	PVP / 3	24	3	Broken nanobelts
S3	$CuSO_4$	0.03	PVP/3	24	5	Irregular flakes and particles
S4	$CuSO_4$	0.03	PVP / 1.5	24	4	Nanobelts with particles
S5	$CuSO_4$	0.03	PVP / 0.3	20	5	Nanobelts with particles
S6	$CuSO_4$	0.03	PVP / 0.3	24	3	Nanobelts
S7	$CuSO_4$	0.03	PVP / 0.3	24	7	Non-uniform nanoparticles
S8	$CuSO_4$	0.03	PVP / 0.3	24	11	Irregular particles
S9	$CuSO_4$	0.03	SDBS / 0.3	20	5	Pieces with particles
S10	$CuSO_4$	0.03	CTAB / 0.3	20	5	Pieces with particles
S11	$CuSO_4$	0.03	−	20	5	Strings with particles
S12	$CuSO_4$	0.075	−	12	5	Irregular particles with microrobs
S13	$Cu(NO_3)_2$	0.075	−	12	5	Irregular particles
S14	$Cu(CH_3COO)_2$	0.075	−	12	5	Nanoparticles
S15	$CuCl_2$	0.075	−	12	5	Irregular particles

0.4494 g (~1.8 mmol) of $CuSO_4·5H_2O$ was simultaneously dissolved in another 30 mL of distilled water at room temperature. The above NH_4VO_3 solution was then added slowly to the $CuSO_4$ solution under a strong magnetic stirring, and then 0.18 g of PVP was finally added into the above mixture, in which the concentrations of Cu^{2+} ($[Cu^{2+}]$), VO_3^- ($[VO_3^-]$), and content of PVP (w(PVP)) were 0.03 mol/L, 0.02 mol/L, and 0.3%, respectively. The pH value of the solution was adjusted to ~3 using sulfuric acid. The resulting suspension was stirred for another 10 min, and then transferred into a Teflon-lined stainless steel autoclave with a volume of 100 mL. After carefully sealed, the autoclave was heated to 180 °C and kept at 180 °C for 24 h, followed by natural cooling in air. The dark green precipitate was collected by centrifugation, washed with water and then freeze-dried in air. The obtained sample with a dark green color was marked as S6 in Table 1, consisting of copper vanadate nanobelts, and then used for further characterization.

2.2 Characterization

2.2.1 Phase composition and morphology

The phase composition was recognized using X-ray diffraction (XRD) patterns, recorded on a D3 X-ray diffractometer equipped with a graphite monochromatized Cu K_α radiation source (λ=1.5406 Å) at a scan rate of 0.05 (°)/s in a 2θ range of 11°−50°. The morphology was observed by scanning electron microscopy (SEM) using a JSM-7001F microscope. The sample was coated with a thin Au film prior to SEM observation.

2.2.2 Electrochemical measurement

To prepare electrodes, the suspensions containing copper vanadate nanocrystals were firstly prepared: 1 mg of the as-obtained copper vanadate nanocrystals and 5 μL of nafion solution (5%) were mixed with 1 mL of *N*, *N*-dimethylformamide (DMF) with a ultra-sonication treatment for 15 min. A glassy carbon electrode (GCE) with a diameter of 3 mm was polished to a mirror finish using polishing papers containing alumina powders with different sizes of firstly 50−70 μm and then 30−50 nm, respectively. The polished GCE was sequentially washed using alcohol and distilled water with an ultrasonic cleaner. Approximately 10 μL of copper vanadate suspensions was finally carefully coated on the surface of the polished GCE. After the solvents evaporated at room temperature, the modified GCEs were used to evaluate their electrochemical properties.

The electrochemical (EC) measurement was performed on an electrochemical working station (model CS310, Wuhan Correst Instruments Co., Ltd., China). The GCEs modified with copper vanadate nanocrystals were served as the working electrodes, and the platinum plate and saturated calomel electrode (SCE) were served as the counter electrode and reference one, respectively. All potentials were with respect to the SCE. Cyclic voltammograms (CVs) were recorded in a potential range of −1.0 V to +1.0 V at a potential scan rate of 50 mV/s in an aqueous solution consisting of 0.1 mol/L KCl and ascorbic acid with a given concentration (0.005−2.0 mmol/L). All electrochemical measurements were carried out at room temperature.

3 Results and discussion

3.1 Effects of copper sources on morphology of copper vanadate nanocrystals

Copper vanadate ($Cu_3V_2O_7(OH)_2·2H_2O$) nanocrystals were synthesized via the reaction between acidic radical copper sources and ammonium met-vanadate under a hydrothermal condition. We firstly checked the effects of acidic radical copper sources on the formation of copper vanadate nanocrystals.

Figure 1 shows the XRD patterns of the samples (S12, S13, S14 and S15 in Table 1) obtained by hydrothermal treatment at 180 °C for 12 h using ammonium met-vanadate and different copper sources ($Cu(CH_3COO)_2·H_2O$, $Cu(NO_3)_2·3H_2O$, $CuCl_2·2H_2O$ or $CuSO_4·5H_2O$) as the reactants (no surfactants and pH=5). As Fig. 1 shows, the characteristic peaks of the four samples are similar, and all the diffraction peaks can be readily indexed to the pure phase of $Cu_3V_2O_7(OH)_2·2H_2O$ with a monoclinic structure (JCPDS card No.80−1170, a=10.607 Å, b=5.864 Å, c=7.214 Å). No other impurities are detected, suggesting that the samples obtained are highly pure. The crystallite diameter of $Cu_3V_2O_7(OH)_2·2H_2O$ nanostructures obtained using the Scherrer equation [33]: $D=K\lambda/\beta\cos\theta$;

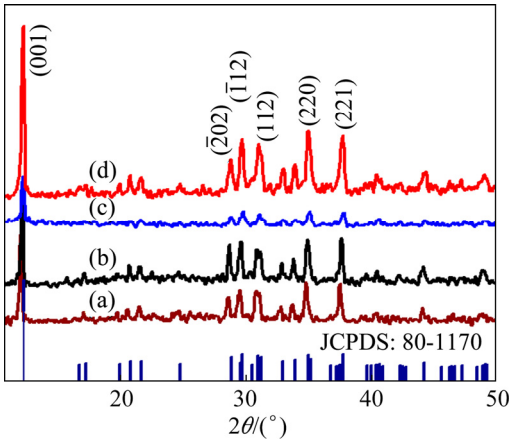

Fig. 1 XRD patterns of $Cu_3V_2O_7(OH)_2·2H_2O$ nanocrystals synthesized using various copper salts as precursors: (a) $CuSO_4·5H_2O$; (b) $Cu(NO_3)_2·3H_2O$; (c) $CuCl_2·H_2O$; (d) $Cu(CH_3COO)_2·H_2O$

where β is the breadth of the observed diffraction line at its half intensity maximum, K is the so-called shape factor, which usually takes a value of about 0.9, and λ is the wavelength of X-ray source used in XRD. Calculated crystalline domain sizes have been found to be 51 nm for sample S14. The peak intensities of sample S14 derived from $Cu(CH_3COO)_2·H_2O$ are stronger than those of the other samples, whereas peak intensities of sample S15 from $CuCl_2·H_2O$ are the weakest ones. The intensities in the XRD peaks indicate that the sample derived from $Cu(CH_3COO)_2·H_2O$ is of higher crystalline degree than that from $CuCl_2·H_2O$.

The morphologies of the $Cu_3V_2O_7(OH)_2·2H_2O$ samples obtained with various copper precursors at 180 °C for 12 h were observed by SEM microscopy. Figure 2 shows the typical SEM images. One can see that the surfaces of $Cu_3V_2O_7(OH)_2·2H_2O$ nanoparticles are greatly affected by the sources of copper salts. Figures 2(a) and (b) show the SEM images of sample S14 derived from $Cu(CH_3COO)_2·H_2O$, and this product is mainly composed of nanoparticles with an average size of ~75 nm. Its corresponding particle-size distribution determined by the Nano Measurer software according the SEM result in Fig. 2(b) is shown in Fig. 3. The Gaussian-fitting curve of the particle-size distribution indicates that the diameters of the nanoparticles range from 55 to 80 nm. NI et al [23,24] reported a similar result, but they used different starting materials and reaction conditions (i.e., V_2O_5, hexamethylenetetramine, $CuSO_4·7H_2O$ or $Cu(NO_3)_2$ and sodium sulfate, at 140 °C for 24 h). The SEM images of the $Cu_3V_2O_7(OH)_2·2H_2O$ samples derived from $CuSO_4$, $Cu(NO_3)_2$, and $CuCl_2$ are shown in Figs. 2(c), (d), and (e), respectively. One can see that these samples mainly consist of nanoparticles with some of one-dimensional species (Fig. 2(c)). According to the SEM images, one can find that copper salts highly influence the morphology of copper vanadate samples. ZHANG et al [34] reported similar influence of copper salts, and thought that the acidity played a key role in the formation of the copper vanadate nanocrystals. The acidity may cause the products to become more agglomerated under special conditions but the purities of them were little affected [29].

3.2 Effects of surfactants and pH values

Various surfactants, including anionic surfactant, cationic surfactant and nonionic surfactant, were used for the growth of copper vanadate nanocrystals. In this work, sodium dodecyl benzene sulfonate (SDBS), hexadecyltrimethy ammonium bromide (CTAB) and

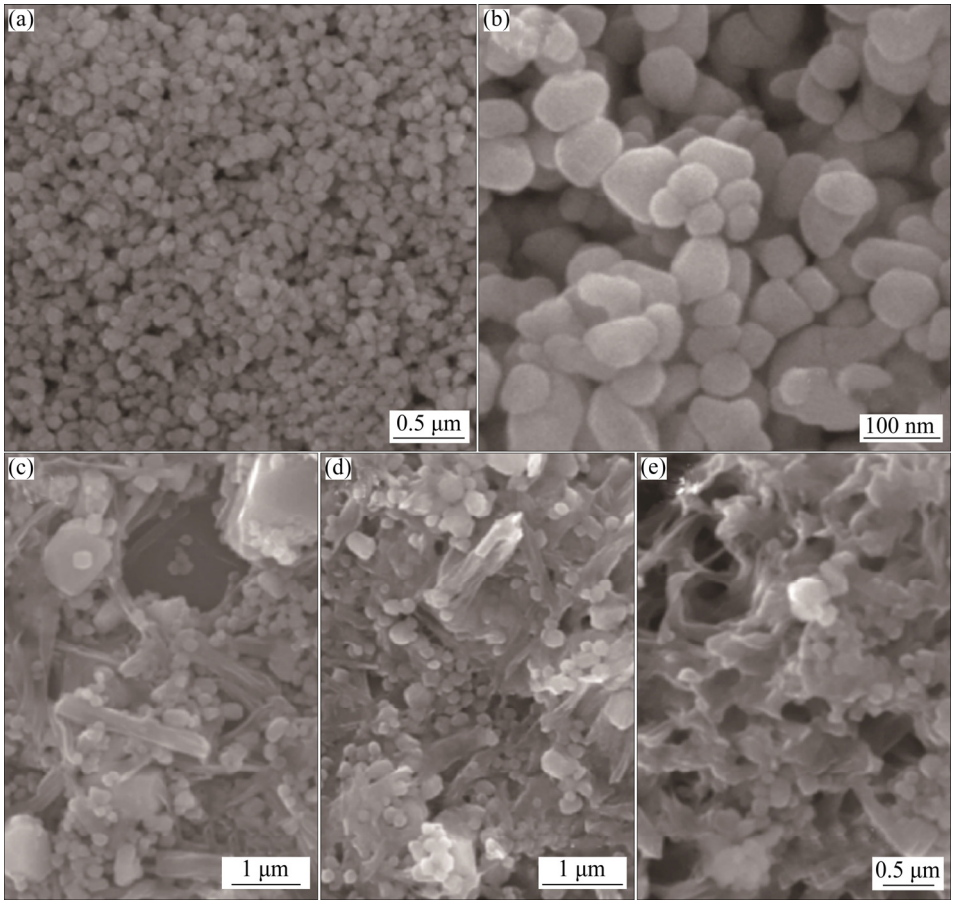

Fig. 2 Typical FE-SEM images of $Cu_3V_2O_7(OH)_2·2H_2O$ nanocrystals using various copper salts as precursors (pH=5, at 180 °C for 12 h): (a, b) $Cu(CH_3COO)_2·H_2O$; (c) $CuSO_4·5H_2O$; (d) $Cu(NO_3)_2·3H_2O$; (e) $CuCl_2·H_2O$

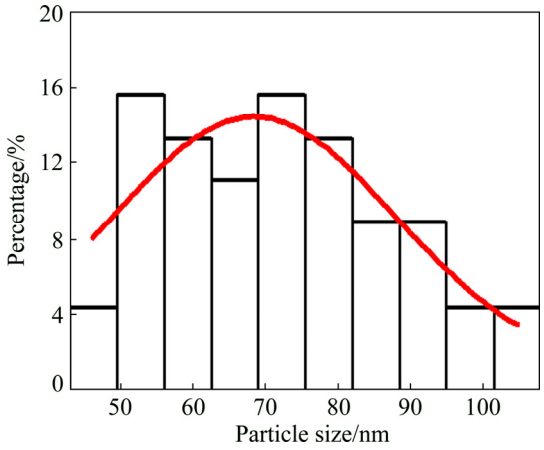

Fig. 3 Particle-size distribution of $Cu_3V_2O_7(OH)_2·2H_2O$ nanocrystals obtained using $Cu(CH_3COO)_2·H_2O$ as precursor (pH=5, at 180 °C for 12 h)

polyvinylpyrrolidone (PVP) were selected as the anionic, cationic and nonionic surfactants, respectively [35−38]. Figure 4 shows the typical SEM images of the $Cu_3V_2O_7(OH)_2·2H_2O$ samples. Figure 4(a) shows the SEM image of the $Cu_3V_2O_7(OH)_2·2H_2O$ sample obtained with PVP, and the sample consists of copper vanadate nanobelts, 30−50 nm in width and more than several micrometers in length. Figures 4(b)−(d) show the SEM images of $Cu_3V_2O_7(OH)_2·2H_2O$ samples obtained with SDBS and CTAB. One can see that the $Cu_3V_2O_7(OH)_2·2H_2O$ nanocrystals obtained with SDBS and CTAB consist of small nanoparticles and some large particles of irregular morphologies.

The effects of the contents of PVP *w*(PVP) and pH values on the morphology of $Cu_3V_2O_7(OH)_2·2H_2O$ nanocrystals were further investigated. Figure 5 shows the typical SEM images of copper vanadate samples obtained using $CuSO_4$ as the Cu source at 180 °C for 24 h with different pH values and PVP concentrations. As Figs. 5(a)−(b) show, the $Cu_3V_2O_7(OH)_2·2H_2O$ samples obtained with conditions of pH=3 and *w*(PVP)= 0.3%−3% take on a belt-like morphology, several-micrometers long and less than 100 nm in the apparent width. The change of the PVP concentration shows a slight impact on their morphology at pH=3, and a higher PVP concentration results in shorter nanobelts [35]. As

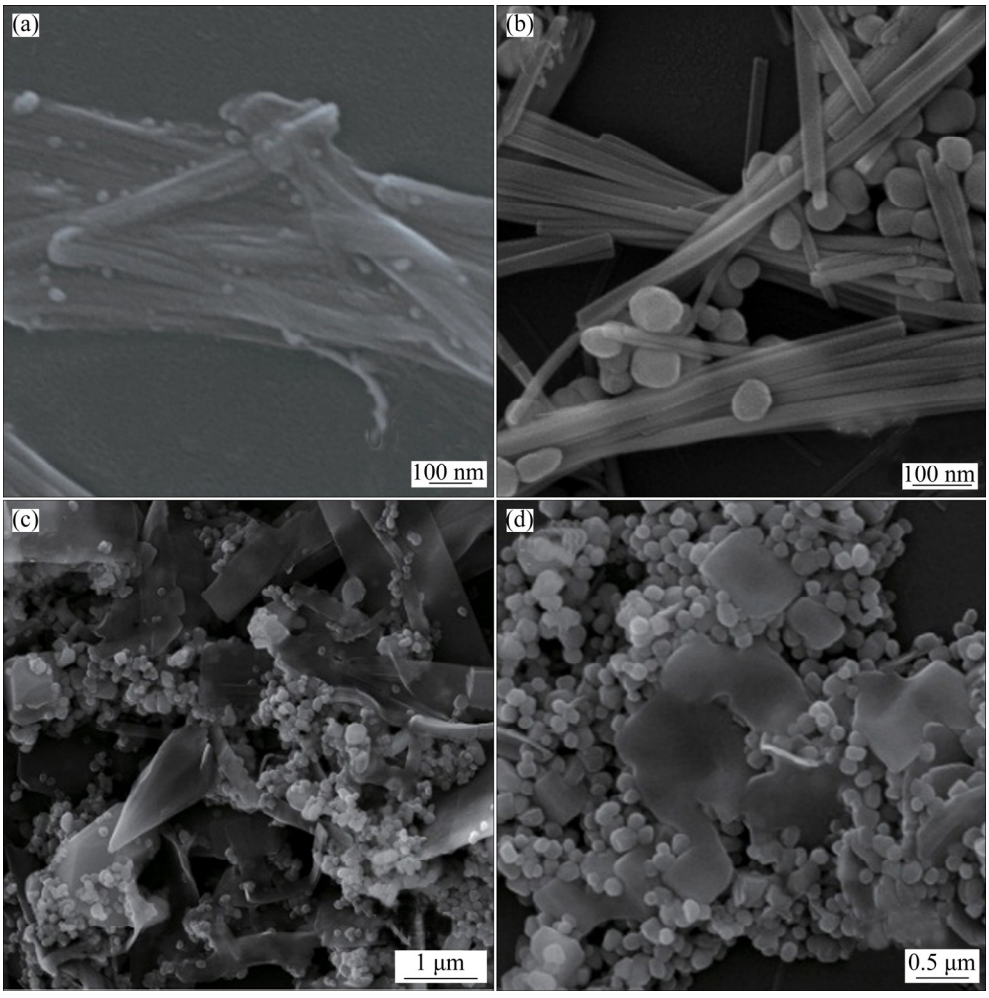

Fig. 4 Typical FE-SEM images of copper vanadate nanocrystals obtained with various surfactants ($CuSO_4$, at 180 °C for 20 h, pH=5, *w*(surfactant)=0.3%): (a) Without surfactant; (b) PVP; (c) CTAB; (d) SDBS

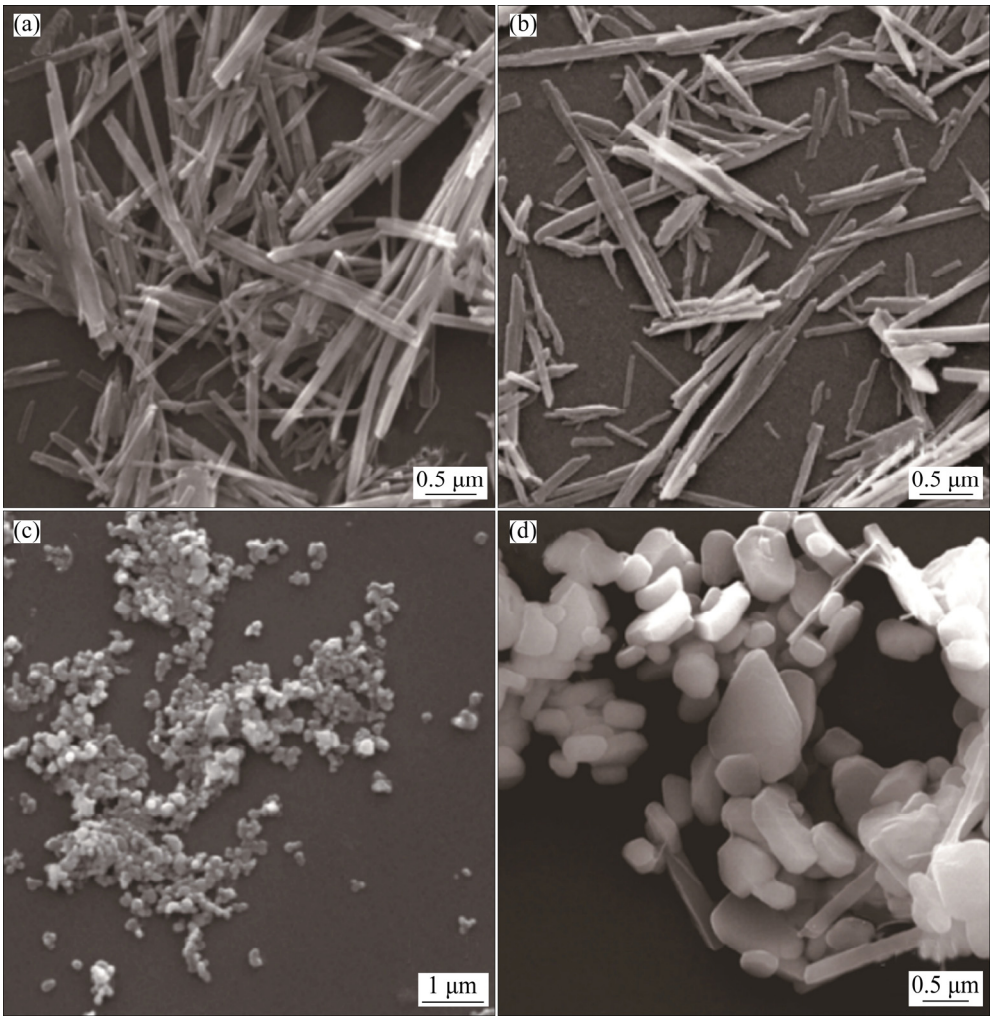

Fig. 5 Typical FE-SEM images of copper vanadate samples obtained using $CuSO_4$ at 180 °C for 24 h with different pH values and PVP contents: (a) pH=3, *w*(PVP)=0.3%; (b) pH=3, *w*(PVP)=3%; (c) pH=7, *w*(PVP)=0.3%; (d) pH=11, *w*(PVP)=0.3%

Figs. 5(a)−(d) show, the pH value is a key factor that influences the morphology of the copper vanadate nanocrystals. When the pH value is 3, uniform nanobelts are obtained (Fig. 5(a)), whereas when the pH value is 7, small nanoparticles with a size range of 50−100 nm are the major products (Fig. 5(c)); when the pH value increases to 11, irregular particles with a sheet-like morphology are formed (Fig. 5(d)).

Figures 6(a)−(b) show the SEM images of $Cu_3V_2O_7(OH)_2{\cdot}2H_2O$ samples obtained when the pH value is 4 and the PVP content is 2.7%. As Figs. 6(a) and (b) show, the product takes on a flower-like morphology, formed by assembling $Cu_3V_2O_7(OH)_2{\cdot}2H_2O$ nanosheets. The diameters of the copper vanadate flowers are 3−5 μm. The formation of flower-like morphology is influenced by the *w*(PVP) and pH values [35]. Figures 6(c) and (d) show the SEM images of the $Cu_3V_2O_7(OH)_2{\cdot}2H_2O$ samples obtained when the pH value was changed to 5 and when the PVP content was changed to 1.5%, respectively. It can be seen that as-obtained samples consist of broken nanorods and particles.

The formation of the $Cu_3V_2O_7(OH)_2{\cdot}2H_2O$ nanocrystals in the present hydrothermal process may be controlled by the synergistic effects of Ostwald ripening and PVP adsorption growth [16,34,35,39,40]. The tiny crystalline nuclei are formed at the initial stage in a supersaturated medium, followed by a crystal growth. With the increase of reaction time, the irregular particles disappear and the long rods grow. Figures 2(c) and 4(a) indicate that the long rods grow at the expense of smaller particles due to the energy difference between them based on the Gibbs−Thompson law [41]. In addition, PVP can act as the rod-like micelle template which plays a critical role in the formation of nanobelts and flowers. The PVP content can influence the length of nanobelts. The pH value is also a vital factor influencing the formation of $Cu_3V_2O_7(OH)_2{\cdot}2H_2O$ nanocrystals. Firstly, the reaction for the formation of $Cu_3V_2O_7(OH)_2{\cdot}2H_2O$ nanocrystals involves H^+ ions; thus when the pH value is

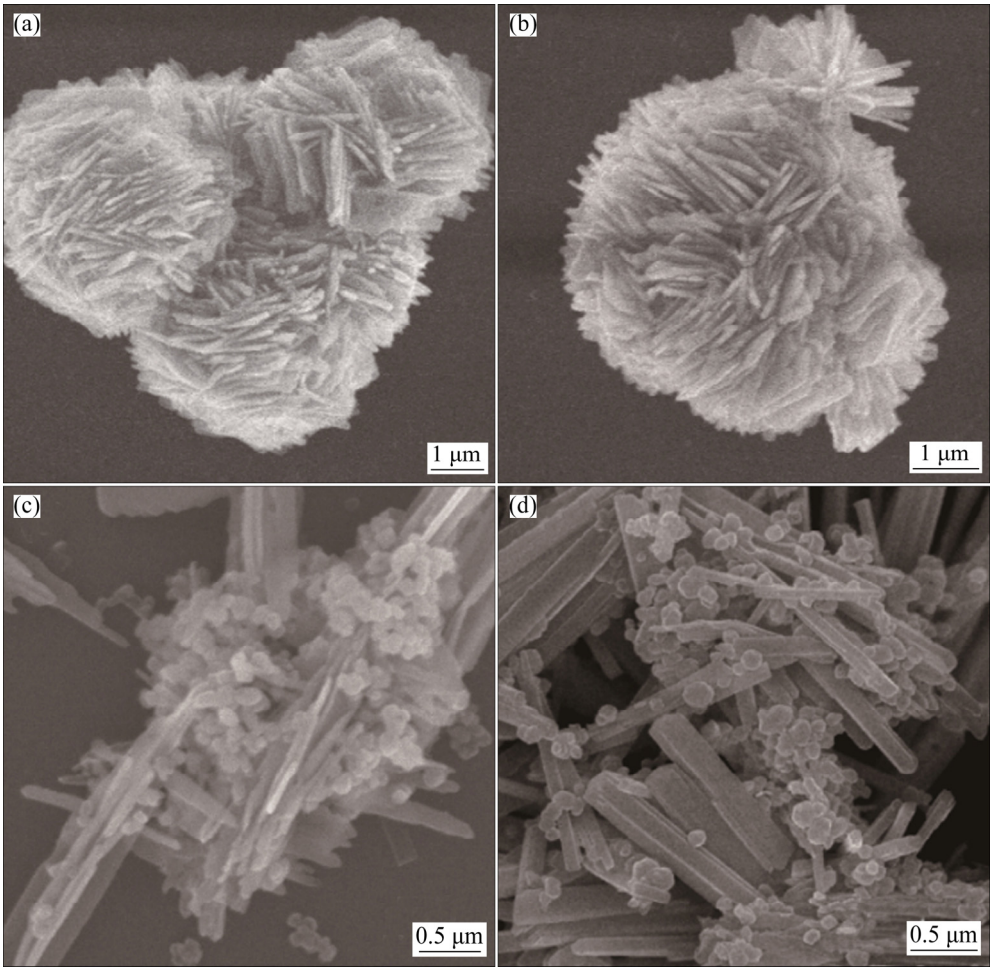

Fig. 6 Typical FE-SEM images of copper vanadate nanocrystals obtained at 180 °C for 24 h (using $CuSO_4$ as raw material): (a, b) pH=4, *w*(PVP)=2.7%; (c) pH=5, *w*(PVP)=2.7%; (d) pH= 4, *w*(PVP)=1.5%

high, i.e., there is a large amount of OH^- ions in the reaction medium, the reaction rate is accelerated greatly and the morphology is hard to control. Secondly, the behavior of the PVP species may greatly change with the change of the pH value, and then the growth of $Cu_3V_2O_7(OH)_2·2H_2O$ nanocrystals is influenced by the pH value.

3.3 Electrochemical performance of copper vanadate nanocrystals

Copper vanadate nanocrystals can act as an electrode-modifying material to accelerate electron transport because of theirs low internal resistance and high discharge capacity [11,16,42]. Ascorbic acid (AA) is sensitive to the physical and chemical properties of the glass carbon electrodes [43,44]. We therefore use copper vanadate nanocrystals to modify the glassy carbon electrodes (GCEs) to modulate the electrochemical response to AA molecules. The as-synthesized $Cu_3V_2O_7(OH)_2·2H_2O$ nanocrystals with various morphologies (i.e., nanoparticles, nanobelts and nanoflowers) were used to modify the GCEs.

Figure 7 shows the electrochemical redox behavior (CV profiles) of ascorbic acid at the interfaces of the $Cu_3V_2O_7(OH)_2·2H_2O$/GCEs in the presence of the ascorbic acid aqueous solution (2 mmol/L). As Fig. 7(a) shows, the bare GCE has no redox peaks. The GCE modified with $Cu_3V_2O_7(OH)_2·2H_2O$ nanobelts (Fig. 7(d)) shows double well-defined redox peaks (i.e., peaks 1 and 1′, peaks 2-3 and 2-3′) with enhanced peak-current intensities, and their anodic and cathodic peak potentials are 0.39 V and −0.17 V, respectively. As Figs. 7(b) and (c) show, the GCEs modified with $Cu_3V_2O_7(OH)_2·2H_2O$ nanoparticles and nanoflowers are lowly sensitive to ascorbic acid, and only one pair of redox peaks are observed in their CVs. This suggests that the $Cu_3V_2O_7(OH)_2·2H_2O$ nanobelts show the best electrochemical activity and the fastest electron transfer under the present neutral conditions. Some similar results with only one pair of relatively weak redox peaks have been reported in the literature [1,2,12]. The electrochemical behavior of the electrodes modified by $CuGeO_3$

nanowires and $CuGeO_3$/polyaniline nanowires to tartaric acid has also shown similar characteristic [45,46]. PEI et al [16] reported that the $Cu_{2.33}V_4O_{11}$ nanobelts/GCEs show two pairs of redox peaks located at different voltages. The difference in the electrochemical redox behavior may result from the difference in the morphology and size of the active materials used to modify their GCEs.

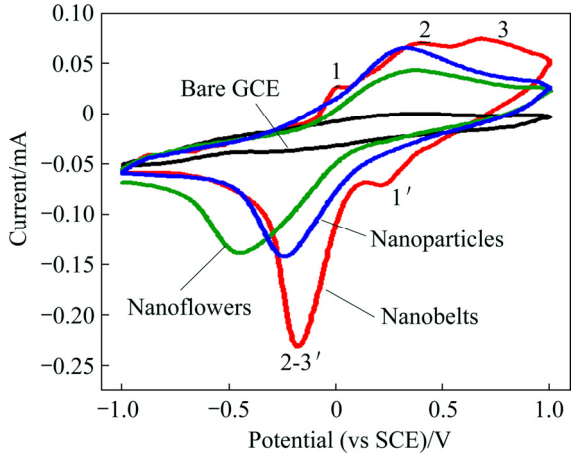

Fig. 7 Cyclic voltammetric profiles of various electrodes at scan rate of 50 mV/s in 0.1 mol/L KCl solution containing 2 mmol/L ascorbic acid

Figure 8 shows the oxidation process of ascorbic acid (AA). AA molecules firstly diffuse to the nearest active sites, and then they are adsorbed onto the surfaces of the copper vanadate nanobelts. The AA molecules adsorbed are finally oxidized to be dehydroascorbic acid with the catalytic effect of the copper vanadate nanobelts. The enhanced electrocatalytical performance of GCEs modified with $Cu_3V_2O_7(OH)_2{\cdot}2H_2O$ nanocrystals can be attributed to the enlarged surface areas of the $Cu_3V_2O_7(OH)_2{\cdot}2H_2O$ nanobelts.

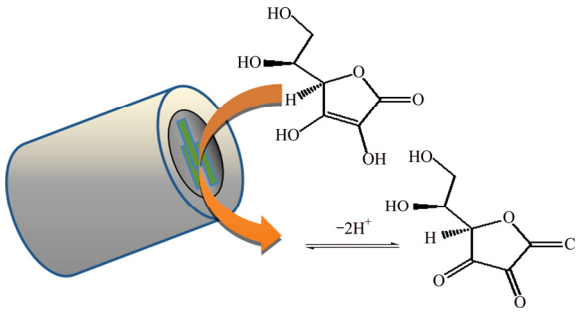

Fig. 8 Schematic of oxydehydrogenation of ascorbic acid oxide

Figure 9 shows the effect of scan rates on the electrochemical behavior of the GCEs modified with $Cu_3V_2O_7(OH)_2{\cdot}2H_2O$ nanobelts in the presence of AA and KCl aqueous solutions ([AA]=2 mol/L and [KCl]= 0.1 mol/L). As Fig. 9(a) shows, when the scan rate increases from 25 mV/s to 125 mV/s, the anodic peak

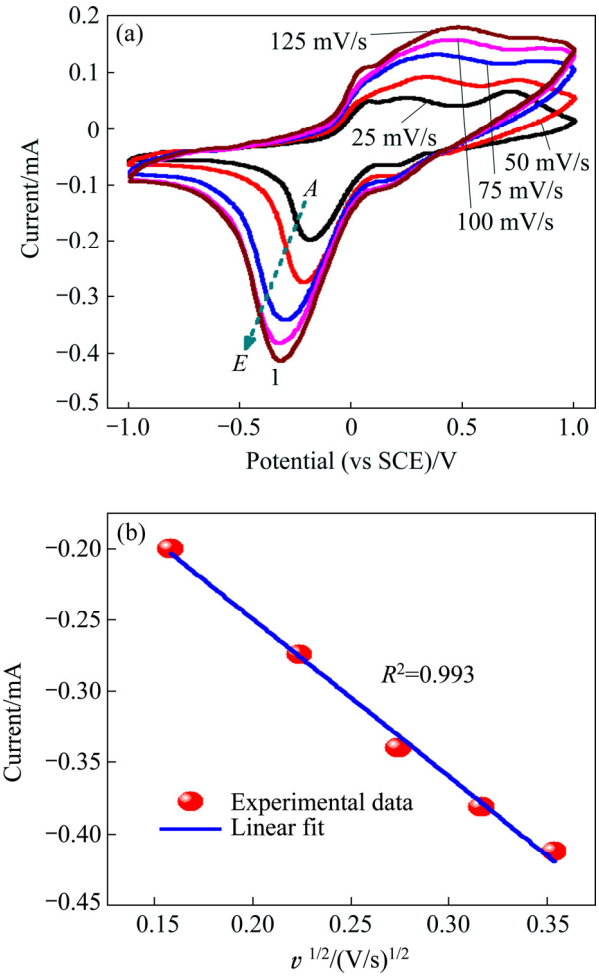

Fig. 9 Cyclic voltammetric profiles of $Cu_3V_2O_7(OH)_2{\cdot}2H_2O$ nanobelts/GCE in 0.1 mol/L KCl solution containing 2 mmol/L ascorbic acid at different scan rates (a) and plot of peak cathodic current (1) versus root square mean of scan rate (b)

potentials shift positively slightly, whereas the cathodic peak potentials move negatively. Figure 9(b) shows the plot of the cathodic peak current versus the square root of the potential scan rate in the range of 25 to 125 mV/s. The obtained linear fitting equation is described as Eq. (1), and its linear correlation coefficient is as high as 0.993. The good linear relationship between the cathodic peak current and the mean square root of the scan rate indicates that the overall oxidation of ascorbic acid at the GCEs modified with $Cu_3V_2O_7(OH)_2{\cdot}2H_2O$ nanobelts is controlled by the diffusion of AA molecules under the present conditions. The peak potentials are not changed obviously, suggesting that the electrode system is reversible to some extent. Thus the diffusion coefficient at room temperature can be calculated using the Randlese−Sevcik equation (Eq. (2)) [7,47,48].

$$I=-0.001v^{1/2}-4.63572\times10^{-5}\ \text{A} \quad (1)$$

$$i_p=(2.69\times10^5)n^{3/2}AD_0^{1/2}C_0^*v^{1/2}\ \text{A} \quad (2)$$

where i_p is the peak current, n is the number of electrons, A (cm^2) is the electrode area, c_0^* (mol/cm^3) is the concentration of ascorbic acid, D_0 (cm^2/s) is the diffusion coefficient, and ν(V/s) is the potential scan rate.

When n, A, c_0^*, D_0 and ν are constants, the $i_p \propto D_0^{1/2}$. It can be concluded that the diffusion coefficient of AA molecules at the $Cu_3V_2O_7(OH)_2{\cdot}2H_2O$ nanobelts/GCE interface is much larger than those of the other two electrodes modified with $Cu_3V_2O_7(OH)_2{\cdot}2H_2O$ nanoparticles and nanoflowers, judged by the larger cathodic peak current (i_p in Fig. 9).

Figure 10(a) shows the CV curves of the GCEs modified with the copper vanadate nanobelts in the presence of 0.1 mol/L KCl aqueous solutions containing ascorbic acid with various concentrations (0.005−2 mmol/L) with a potential scan rate of 50 mV/s. Figure 10(b) shows the plot of the cathodic peak current versus the AA concentration. One sees that the absolute values of the peak currents increase linearly with the increase in AA concentrations. The linear fitting equation obtained according to the parameters of peak 1 is shown as Eq. (3), where c (mmol/L) is the concentration of ascorbic acid, with a linear correlation coefficient (R^2) as high as 0.994 in the [AA] range of 0.005−2 mmol/L. The comparison of the liner range of the electrochemical determination of ascorbic acid with other electrodes and modifiers is shown in Table 2, indicating that every research done in recent years had their own characteristics. The copper vanadate nanobelts obtained in the present work can be used as a potential sensing platform for electrochemically quantitative detection of ascorbic acid.

$$I=-1.02(4)\times10^{-4}c-6.9(3)\times10^{-5}\ \text{A} \quad (3)$$

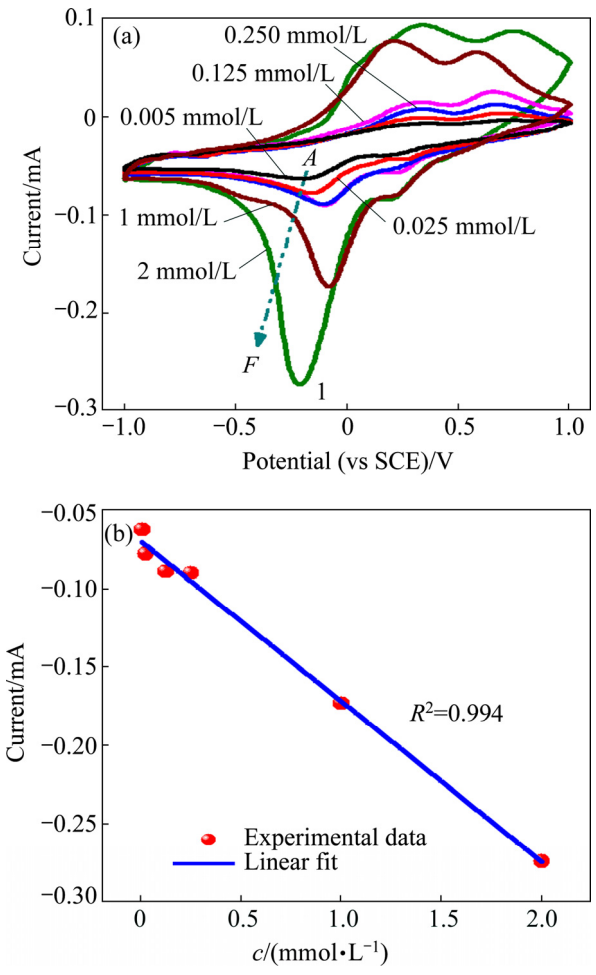

Fig. 10 Cyclic voltammetric profiles of copper vanadate nanobelts modified GCE in 0.1 mol/L KCl solution containing ascorbic acid with different concentrations with scan rate of 50 mV/s (a), plot of the peak cathodic currents (1) versus ascorbic acid concentrations (b)

Table 2 Comparison of liner range of electrochemical determination of ascorbic acid other researches

Electrode	Modifier	Linear range/ (mmol·L^{-1})	Time/ Ref.
Au	PAH/polysaccharide films confined $Fe(CN)_6^{3-}$	1−50	2007/[49]
Carbon nanotube paste electrode	Silver nanoparticles	0.03−2	2009/[50]
Glassy carbon electrode	Pd nanowire	0.025−0.9	2010/[51]
Glassy carbon electrode	Palladium nanoparticles supported on graphene oxide	0.02−2.28	2012/[52]
3D graphene foam	CuO nanoflowers	0.00043−0.2	2014/[2]
Glassy carbon electrode	Hierarchical nanoporous (HNP) PtTi alloy	0.2−1	2016/[53]
Glassy carbon electrode	$Cu_3V_2O_7(OH)_2{\cdot}2H_2O$ nanobelts	0.005−2	This work

The electrochemical behavior of the GCEs modified with the copper vanadate nanobelts in the presence of ascorbic acid aqueous solution was also investigated under various pH conditions, e.g., in the electrolytes including NaOH (pH=12) and H_2SO_4 (pH=2). Figure 11 shows the typical results. The ascorbic acid molecules in the acidic or alkaline conditions have no redox peaks, indicating that the [H^+] concentration in the solution influences the oxidation of ascorbic acid. Ascorbic acid is an acid relatively stable under the acidic condition, less prone to oxidation−reduction reactions. AA is not stable in the alkaline environment, leading to the irreversibility of oxidation−reduction reactions. Therefore, the determination of AA using the GCEs modified with the copper vanadate nanobelts should be limited to a neutral condition.

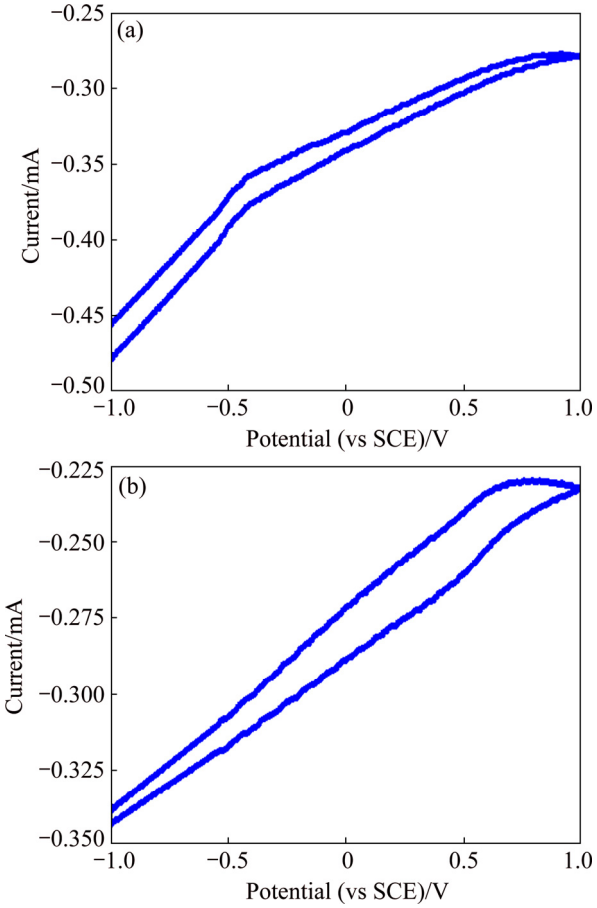

Fig. 11 Cyclic voltammetric profiles of copper vanadate nanobelts modified GCE electrodes in H_2SO_4 (a) and NaOH (b) solutions containing 2 mmol/L ascorbic acid with scan rate of 50 mV/s

4 Conclusions

1) The $Cu_3V_2O_7(OH)_2·2H_2O$ nanocrystals with various morphologies (e.g., nanoparticles, nanobelts and nanoflowers) have been synthesized via a hydrothermal process by adjusting the experimental conditions. $Cu(CH_3COO)_2·H_2O$ is the suitable copper source for the synthesis of nanoparticles. $Cu_3V_2O_7(OH)_2·2H_2O$ nanobelts are synthesized using $CuSO_4·5H_2O$ as the copper source with PVP (0.3%−3%) and pH=3. The $Cu_3V_2O_7(OH)_2·2H_2O$ nanoflowers are formed under the condition of pH=4 and *w*(PVP)=2.7%.

2) The GCEs modified with the $Cu_3V_2O_7(OH)_2·2H_2O$ nanobelts show higher electrochemical activity to ascorbic acid than those modified with $Cu_3V_2O_7(OH)_2·2H_2O$ nanoparticles and nanoflowers. The absolute values of the peak currents in the CVs increase linearly with the ascorbic acid concentrations in the range of 0.005−2 mmol/L.

3) The $Cu_3V_2O_7(OH)_2·2H_2O$ nanobelts can be a promising candidate of electrochemically active material to modify glassy carbon electrodes that are applied in electrochemical determination of ascorbic acid or other organic molecules qualitatively or quantitatively.

References

[1] KARIMI-MALEH H, MOAZAMPOUR M, YOOSEFIAN M, SANATI A L, TAHERNEJAD-JAVAZMI F, MAHANI M. An electrochemical nanosensor for simultaneous voltammetric determination of ascorbic acid and sudan I in food samples [J]. Food Analytical Methods, 2014, 7(10): 2169−2176.

[2] MA Y, ZHAO M, CAI B, WANG W, YE Z, HUANG J. 3D graphene foams decorated by CuO nanoflowers for ultrasensitive ascorbic acid detection [J]. Biosensors and Bioelectronics, 2014, 59: 384−388.

[3] LEONARDI S G, ALOISIO D, DONATO N, RATHI S, GHOSH K, NERI G. Electrochemical sensing of ascorbic acid by a novel manganese(III) complex [J]. Materials Letters, 2014, 133: 232−235.

[4] SAKIRA A K, SOMC I T, ZIEMONS E, DEJAEGHER B, MERTENS D, HUBERT P, KAUFFMANN J. Determination of arsenic (III) at a nanogold modified solid carbon paste electrode [J]. Electroanalysis, 2015, 27(2): 309−316.

[5] HUANG X, LI Y, CHEN Y, WANG L. Electrochemical determination of nitrite and iodate by use of gold nanoparticles/ poly(3-methylthiophene) composites coated glassy carbon electrode [J]. Sensors and Actuators B: Chemical, 2008, 134(2): 780−786.

[6] IDRIS A O, MABUBA N, AROTIBA O A. Electroanalysis of selenium in water on an electrodeposited gold-nanoparticle modified glassy carbon electrode [J]. Journal of Electroanalytical Chemistry, 2015, 758: 7−11.

[7] SONG M J, HWANG S W, WHANG D. Non-enzymatic electrochemical CuO nanoflowers sensor for hydrogen peroxide detection [J]. Talanta, 2010, 80(5): 1648−1652.

[8] PEI L Z, LIU H D , LIN N, XIE Y K, CAI Z Y. Electrochemical analysis of cyanuric acid using polyaniline/$CuGeO_3$ nanowires as electrode modified materials [J]. Current Pharmaceutical Analysis, 2015, 11(1): 16−24.

[9] LI H, WANG Y, YE D, LUO J, SU B, ZHANG S, KONG J. An electrochemical sensor for simultaneous determination of ascorbic acid, dopamine, uric acid and tryptophan based on MWNTs bridged mesocellular graphene foam nanocomposite [J]. Talanta, 2014, 127: 255−261.

[10] QIAN J, YANG X, YANG Z, ZHU G, MAO H, WANG K. Multiwalled carbon nanotube@ reduced graphene oxide nanoribbon heterostructure: Aynthesis, intrinsic peroxidase-like catalytic activity, and its application in colorimetric biosensing [J]. Journal of Materials Chemistry B, 2015, 3(8): 1624−1632.

[11] SIVAKUMAR V, SURESH R, GIRIBABU K, MANIGANDAN R, MUNUSAMY S, KUMAR S P, MUTHAMIZH S, NARAYANAN V. Copper vanadate nanoparticles: Synthesis, characterization and its electrochemical sensing property [J]. Materials in Electronics, 2014, 25(3): 1485−1491.

[12] CHANG K C, CHU C M, CHANG C H, CHENG H T, HSU S C, LAN C C, CHEN H H, PENG Y Y,YEH J M. Photoisomerization of electroactive polyimide/multiwalled carbon nanotube composites on the effect of electrochemical sensing for ascorbic acid [J]. Polymer International, 2015, 64(3): 373−382.

[13] MANDAL D, MONDAL S, SENAPATI D, SATPATI B, SANGARANARAYANAN M V. Charge density modulated shape-dependent electrocatalytic activity of gold nanoparticles for the oxidation of ascorbic acid [J]. The Journal of Physical Chemistry C, 2015, 119(40): 23103−23112.

[14] AFONSO R, EISELE A P P, SERAFIM J A, LUCILHA A C, DUARTE E H, TARLEY C R T, SARTORI E R, DALL'ANTONIA L H. $BiVO_4$-Bi_2O_3/ITO electrodes prepared by layer-by-layer:

Application in the determination of atenolol in pharmaceutical formulations and urine [J]. Journal of Electroanalytical Chemistry, 2016, 765: 30−36.

[15] PEI L, LIU H, XIE Y, CAI Z. Electrochemical determination of L-cysteine by cyclic voltammetry using calcium vanadate nanorod modified glassy carbon electrode [J]. Journal of Bionanoscience, 2014, 8(2): 146−150.

[16] PEI L, LIN N, WEI T, LIU H, YU H, Formation of copper vanadate nanobelts and their electrochemical behaviors for the determination of ascorbic acid [J]. Journal of Materials Chemistry A, 2015, 3(6): 2690−2700.

[17] PEI L, PEI Y, XIE Y, FAN C, LI D, ZHANG Q. Formation process of calcium vanadate nanorods and their electrochemical sensing properties [J]. Journal of Materials Research, 2012, 27(18): 2391−2400.

[18] PEI L Z, PEI Y, XIE Y, FAN C, ZHANG Q. Formation mechanism of manganese vanadate microtubes and their electrochemical sensing properties [J]. International Journal of Materials Research, 2013, 104(12): 1267−1273.

[19] WEI Y J, NAM K W, CHEN G, RYU C W, KIM K B. Synthesis and structural properties of stoichiometric and oxygen deficient CuV_2O_6 prepared via co-precipitation method [J]. Solid State Ionics, 2005, 176: 2243−2249.

[20] HU F, LI M, WEI Y, DU F, CHEN G, WANG C. Synthesis and electrochemical properties of highly crystallized CuV_2O_6 nanowires [J]. Chemical Research in Chinese Universities, 2015, 31(5): 708−711.

[21] CAO X Y, XIE J G, ZHAN H, ZHOU Y H. Synthesis of CuV_2O_6 as a cathode material for rechargeable lithium batteries from V_2O_5 gel [J]. Materials chemistry and physics, 2006, 98(1): 71−75.

[22] HU W, DU X, WU Y, WANG L. Novel ε-$Cu_{0.95}V_2O_5$ hollow microspheres and α-CuV_2O_6 nanograins: Facile synthesis and application in lithium-ion batteries [J]. Journal of Power Sources, 2013, 237: 112−118.

[23] NI S, HE D, YANG X, LI T. Hydrothermal synthesis of $Cu_3(OH)_2V_2O_7{\cdot}nH_2O$ nanoparticles and its application in lithium ion battery [J]. Journal of Alloys and Compounds, 2011, 509(8): L142−L144.

[24] NI S, WANG X, ZHOU G, YANG F, WANG J, HE D. Hydrothermal synthesis and magnetic property of $Cu_3(OH)$ $V_2O_7{\cdot}nH_2O$ [J]. Materials Letters, 2010 64(4): 516−519.

[25] MELGHIT K, WEN L S. The effect of starting materials on the morphology and particle size of copper pyrovanadate $Cu_3V_2O_7(OH)_2{\cdot}2H_2O$ [J]. Ceramics international, 2005, 31(2): 223−225.

[26] GHIYASIYAN-ARANI M, MASJEDI-ARANI M, GHANBARI D, BAGHERI S, SALAVATI-NIASARI M. Novel chemical synthesis and characterization of copper pyrovanadate nanoparticles and its influence on the flame retardancy of polymeric nanocomposites [J]. Scientific Reports, 2016, 6.

[27] GHIYASIYAN-ARANI M, MASJEDI-ARANI M, SALAVATI-NIASARI M. Novel Schiff base ligand-assisted in-situ synthesis of $Cu_3V_2O_8$ nanoparticles via a simple precipitation approach [J]. Journal of Molecular Liquids, 2016, 216: 59−66.

[28] GHIYASIYAN-ARANI M, MASJEDI-ARANI M, SALAVATI-NIASARI M. Facile synthesis, characterization and optical properties of copper vanadate nanostructures for enhanced photocatalytic activity [J]. Journal of Materials Science: Materials in Electronics, 2016, 27(5): 4871−4878.

[29] MAZLOOM F, MASJEDI-ARANI M, GHIYASIYAN-ARANI M, SALAVATI-NIASARI M. Novel sodium dodecyl sulfate-assisted synthesis of $Zn_3V_2O_8$ nanostructures via a simple route [J]. Journal of Molecular Liquids, 2016, 214: 46−53.

[30] MAZLOOM F, MASJEDI-ARANI M, SALAVATI-NIASARI M. Novel size-controlled fabrication of pure $Zn_3V_2O_8$ nanostructures via a simple precipitation approach [J]. Journal of Materials Science: Materials in Electronics, 2016, 27(2): 1974−1982.

[31] MAZLOOM F, MASJEDI-ARANI M, SALAVATI-NIASARI M. Controllable synthesis, characterization and photocatalytic studies on cadmium vanadate nanostructures [J]. Journal of Molecular Liquids, 2016, 220: 566−572.

[32] GHIYASIYAN-ARANI M, MASJEDI-ARANI M, SALAVATI-NIASARI M. Simple precipitation synthesis of pure $Cu_3V_2O_8$ nanoparticles and investigation of their optical properties [J]. Journal of Nanostructures, 2015, 5(4): 437−441.

[33] MASJEDI-ARANI M, SALAVATI-NIASARI M. A simple sonochemical approach for synthesis and characterization of Zn_2SiO_4 nanostructures [J]. Ultrasonics Sonochemistry, 2016, 29: 226−235.

[34] ZHANG S, CI L, LIU H. Synthesis, characterization, and electrochemical properties of $Cu_3V_2O_7(OH)_2{\cdot}2H_2O$ nanostructures [J]. The Journal of Physical Chemistry C, 2009, 113(20): 8624−8629.

[35] MURPHY C J, JANA N R. Controlling the aspect ratio of inorganic nanorods and nanowires [J]. Advanced Materials, 2002, 14: 80−82.

[36] SUN Y, MAYERS B, HERRICKS T, XIA Y. Polyol synthesis of uniform silver nanowires: A plausible growth mechanism and the supporting evidence [J]. Nano letters, 2003, 3(7): 955−960.

[37] ZHANG Shui-rong, HU, Zhi-biao, LIU Kai-yu, LIU Yan-zhen, HE Fang, XIE Qing-liang. Synthesis and characterization of porous cobalt oxide/copper oxide nanoplate as novel electrode material for supercapacitors [J]. Transactions of Nonferrous Metals Society of China, 2015, 25(12): 4054−4062.

[38] SHEN Xiang, WANG Yan-xin, YANG Xiang, XIA Yong, ZHUANG Jian-feng, TANG Pei-duo. Megahertz magneto-dielectric properties of nanosized NiZnCo ferrite from CTAB-assisted hydrothermal process [J]. Transactions of Nonferrous Metals Society of China, 2015, 19(6): 1588−1592.

[39] LI G, WU W, ZHANG C, PENG H, CHEN K. Synthesis of ultra-long single crystalline CuV_2O_6 nanobelts [J]. Materials Letters, 2010, 64(7): 820−823.

[40] LI R, LUO Z, PAPADIMITRAKOPOULOS F. Redox-assisted asymmetric ostwald ripening of CdSe dots to rods [J]. Journal of the American Chemical Society, 2006, 128(19): 6280−6281.

[41] MITCHELL J, WEBBER J B W, STRANGE J H. Nuclear magnetic resonance cryoporometry [J]. Physics Reports, 2008, 461(1): 1−36.

[42] JIA B, QIN M, ZHANG Z, ZHANG L, LIU Y, CHU A, QU X. Hierarchical $Cu_4V_{2.15}O_{9.38}$ superstructures assembled by single-crystalline rods: their synthesis, characteristics and electrochemical properties [J]. RSC Advances, 2014, 4: 62237−62243.

[43] FAGAN D T, HU I F, KUWANA T. Vacuum heat-treatment for activation of glassy carbon electrodes [J]. Analytical Chemistry, 1985, 57(14): 2759−2763.

[44] ENGSTROM R C, STRASSER V A. Characterization of electrochemically pretreated glassy carbon electrodes [J]. Analytical Chemistry, 1984, 56(2): 136−141.

[45] CAI Z Y, PEI L Z, YANG Y, PEI Y Q, FAN C G, FU D G. Electrochemical behavior of tartaric acid at $CuGeO_3$ nanowire modified glassy carbon electrode [J]. Journal of Solid State Electrochemistry, 2012,16(6): 2243−2249.

[46] CAI Z Y, PEI L Z, PEI Y Q, XIE Y, FAN C G, FU D G. $CuGeO_3$/polyaniline nanowires and their electrochemical responses for tartaric acid [J]. Measurement Science and Technology, 2012, 23(11): 115701−115707.

[47] TANAKA N, TAMAMUSHI R. Kinetic parameters of electrode reactions [J]. Electrochimica Acta, 1964, 9(7): 963−989.

[48] BI Z H, PARANTHAMAN M P, GUO B K , UNOCIC R R, MEYER III H M, BRIDGES C A, SUN X G, DAI S. High performance Cr, N-codoped mesoporous TiO_2 microspheres for lithium-ion batteries

[J]. Journal of Materials Chemistry A, 2014, 2: 1818−1824.
[49] WANG B, NOGUCHI T, ANZAI J. Layer-by-layer thin film-coated electrodes for electrocatalytic determination of ascorbic acid [J]. Talanta, 2007, 72(2): 415−418.
[50] TASHKHOURIAN J, NEZHAD M R H, KHODAVESI J, JAVADI. S. Silver nanoparticles modified carbon nanotube paste electrode for simultaneous determination of dopamine and ascorbic acid [J]. Journal of Electroanalytical Chemistry, 2009, 633(1): 85−91.
[51] WEN D, GUO S, DONG S, WANG E. Ultrathin Pd nanowire as a highly active electrode material for sensitive and selective detection of ascorbic acid[J]. Biosensors and Bioelectronics, 2010, 26(3): 1056−1061.
[52] WU G, WU Y, LIU X, RONG M, CHEN X, CHEN X. An electrochemical ascorbic acid sensor based on palladium nanoparticles supported on graphene oxide [J]. Analytica Chimica Acta, 2012, 745: 33−37.
[53] ZHAO D, YU G, TIAN K, XU C. A highly sensitive and stable electrochemical sensor for simultaneous detection towards ascorbic acid, dopamine, and uric acid based on the hierarchical nanoporous PtTi alloy [J]. Biosensors and Bioelectronics, 2016, 82: 119−126.

形貌可控钒酸铜纳米晶的水热合成及其电化学传感性能

韩桂洪[1]，杨淑珍[1]，黄艳芳[1]，杨 晶[2]，柴文翠[1]，张 锐[2]，陈德良[2]

1. 郑州大学 化工与能源学院，郑州 450001；
2. 郑州大学 材料科学与工程学院，郑州 450001

摘 要：形貌可控钒酸铜纳米晶在电化学传感应用上具有非常重要的意义。采用简便的水热合成方法，制备出一系列具有不同形貌的的钒酸铜纳米晶(纳米颗粒，纳米带和纳米花)。采用 XRD、SEM 和循环伏安法(CV)等测试技术，对各种钒酸铜纳米晶产物的物相组成、形貌和电化学性能进行表征。结果表明，$Cu_3V_2O_7(OH)_2\cdot 2H_2O$ (CVOH)晶体的形貌可以通过改变铜盐、表面活性剂种类以及溶液 pH 值进行调控。采用 CVOH 纳米晶作为活性材料修饰玻碳电极(GCEs)发现，电极对抗坏血酸的响应性能增强。比较三种不同形貌的钒酸铜纳米晶，纳米带状对电极的增强效应最显著。钒酸铜纳米带修饰 GCEs 电化学感应抗坏血酸，其 CV 的峰值电流与其浓度呈正比。因此，CVOH 纳米晶体可作为检测抗坏血酸的电化学活性材料。

关键词：钒酸铜纳米晶；水热合成；电化学传感；抗坏血酸

(Edited by Yun-bin HE)